Optics Communications
Manuscript Draft

Manuscript Number: PV-750

Title: Broadband unidirectional near-zero reflection induced by logical combination of parity-time symmetric photonic crystal

Article Type: Research Paper

Keywords: Aperiodic; Photonic crystal; PT-symmetry; Exceptional point

Abstract: The aperiodic photonic crystal is derived by the "OR" Boolean algorithm of two periodic photonic crystals with slightly different periods, which shows broadband reflection features. Inspired by this, in this paper we propose an aperiodic photonic crystal with PT-symmetry to investigate the broadband unidirectional reflection behavior. By analyzing the scattering matrix of the proposed structure, we reveal that the broadband near-zero reflection phenomenon is induced by the interaction of multiple exceptional points. The underlying physics of this phenomenon is exploited by investigating the electric field distribution at exceptional points. Furthermore, an interface state is also found to locate at the loss/gain boundary of PT-symmetric materials. The broadband (~1200 nm) near-zero reflection phenomenon with unidirectional property is first discussed in the PT-symmetric structure, which gives us hints for further investigations of unidirectional reflection in non-Hermitian systems.

Broadband unidirectional near-zero reflection induced by logical combination of parity-time symmetric photonic crystal

YUE FEI, YOU-WEN LIU*, DA-XING DONG, YONG-QING FAN, AND YANG-YANG FU†

College of Science, Nanjing University of Aeronautics and Astronautics, Nanjing 210016, China

**ywliu@nuaa.edu.cn †yyfu@nuaa.edu.cn*

Abstract: The aperiodic photonic crystal is derived by the "OR" Boolean algorithm of two periodic photonic crystals with slightly different periods, which shows broadband reflection features. Inspired by this, in this paper we propose an aperiodic photonic crystal with PT-symmetry to investigate the broadband unidirectional reflection behavior. By analyzing the scattering matrix of the proposed structure, we reveal that the broadband near-zero reflection phenomenon is induced by the interaction of multiple exceptional points. The underlying physics of this phenomenon is exploited by investigating the electric field distribution at exceptional points. Furthermore, an interface state is also found to locate at the loss/gain boundary of PT-symmetric materials. The broadband (~1200 nm) near-zero reflection phenomenon with unidirectional property is first discussed in the PT-symmetric structure, which gives us hints for further investigations of unidirectional reflection in non-Hermitian systems.

Keyword: Aperiodic; Photonic crystal; PT-symmetry; Exceptional point

1. Introduction

Photonic crystal (PC) is an emerging field in optics and has been intensively investigated over the past thirty years [1]. In analogy to traditional semiconductor materials with electron bandgaps, there appears a frequency range where no electromagnetic eigenmode exists in PC, which is also called photonic bandgaps (PBGs). Light with frequency locating in PBG undergoes exponential decay inside the photonic structure, and shows a total reflection in their spectra [2]. Till now, a large number of PC-based proposals have been put forward, such as slow light [3], filter [4], waveguide [5] and topological design [6]. With the advancement of theory and experiments, quasiperiodic PCs (QPCs) and aperiodic PCs (APCs) are introduced to enrich the spectrum of periodic PCs [7]. Short after the uncovering of the quasicrystals in the field of crystallography in 1984 [8], QPC with the Fibonacci sequence was discussed by Kohmoto comprehensively [9]. Compared with periodic PCs showing only single basic bandgap in its spectrum, QPCs and APCs show diverse stopbands and self-similarity in their band structures. In the beginning, QPCs are generated mainly by substitution rules following different sequences, such as Fibonacci sequence, Cantor sequence and Thue-Morse structure [10], et al. All of them show multiple stopbands in their spectra. Recently, researchers proposed a new kind of aperiodic photonic crystal, which is also called dual-periodic photonic crystals. As the name suggests, this kind of PC is constructed by two different periodic PCs via applying distinct mathematical algorithms. These algorithms can be binary Boolean operation [11], step functions [12] and some other quantitative methods. Compared with ordinary photonic structures, dual-periodic PCs possess more advantageous properties, such as adjustable bandgaps, broadband slow modes and predesigned optical Tamm states [13]. For example, the logical combined photonic crystal (LCPC), which is constructed by the combination of two periodic photonic crystals respecting the Boolean operation "OR", shows broadband features and flat band in its spectrum [11,14]. By applying "OR" operation in PCs, multiple coupling of Bloch modes could be induced, and thus broadband reflection appears. As a fast-growing topic in optics, aperiodic photonic structure thrives and flourishes, and opens an avenue for complicated photonic design.

PT对称的概述

Parity-time (PT) symmetric structure is a popular project in the scope of metamaterials [15]. In quantum physics, only Hermitian Hamiltonian is believed to possess real spectrum with observable momentum, while the eigenvalues of non-Hermitian Hamiltonian are complex, which indicate unobservable momentum. However, Bender showed that real spectra can also exist in non-Hermitian Hamiltonians as long as they respect PT-symmetry [16]. Another intriguing characteristic of PT-symmetric structure is the spontaneous symmetry-breaking point, which is also called exceptional point (EP). The eigenvalues of the PT-symmetric structure and their corresponding eigenvectors coalesce simultaneously at EPs, and a phase transition emerges. In optics, the non-Hermitian Hamiltonian of a photonic configuration conserves PT-symmetry by applying judicious modulation of index distribution on it (viz. n (z) = n*(-z)). In other words, the real part of the refractive index is an even function along the z-axis while the imaginary part obeys odd function. The introduced optical gain and loss create a new category of artificial materials with new optical properties. Till now, an abundant of researches related to PT-symmetry have been conducted in optics, such as optical solitons in PT potential [17], photonic crystal with PT-symmetry [18], and zero index metamaterial with PT-symmetry [19,20]. Devices obeying PT-symmetry exhibit many counter-intuitive phenomena, for instance, unidirectional invisibility [21,22], asymmetric diffraction [23] and splitting exceptional point [24]. In particular, unidirectional reflection effect has been successfully demonstrated in experiments [22], and serves as a modification tool in designing novel photonic devices. However, unidirectional reflection effect in almost all PT-symmetric structures only works in a narrow band of frequencies, hindering its application in broadband photonic devices.

PT对称应用

Inspired by the broadband features in aperiodic photonic crystals formed by logical "OR" combination, we investigate the scattering spectrum of the PT-symmetric LCPC and find a unidirectional near-zero reflection phenomenon over a broad wavelength range for about 1200 nm. The spectrum of the PT-symmetric structure is calculated by the transfer matrix method, and shows asymmetric reflection spectrum for lights incident from different directions. When the light is incident from the loss side, the broadband near-zero reflection (BNZR) appears, while BNZR disappears in the opposite direction. The scattering matrix for the PT-symmetric configuration is computed and compared with the periodic PCs to uncover the reason for the broadband invisibility. Furthermore, we investigated the electric field distribution for different wavelengths of EPs to get a further understanding of the BNZR phenomenon. The idea of combining two-periodic PCs with PT modification is first introduced in the field of photonic crystals, and this attempt may give hints to facilitate further PT-symmetric photonic designs.

2. Theory model

Firstly, we construct two traditional periodic photonic crystals PC_1 and PC_2. As shown in Fig. 1(a), PC_1 is made up of two alternative dielectric materials *A* and *B*, with refractive index n_A and n_B ($n_A > n_B$). The period and filling ratio of PC_1 are set as *p* and f_1. Similarly, by keeping the thickness of the high refractive index layer *A* unchanged, we enlarged the length of PC_1 by *r* to get PC_2, where *r* is a rational number, and the period of PC_2 would be *rp*. In Fig. 1(a), we treat layer *A* as "1" and layer *B* as "0". Like binary Boolean operation, the "OR" operation in photonic crystals will get n_A when one of the two material indexes equal to n_A; and get n_B when both the indexes equal to n_B. The schematic illustration of the configuration of LCPCs [11] is given in the lower parts in Fig. 1(a). Now, we get the logical combination of the two-period photonic crystals with slightly different periodicities. Clearly, the length of the LCPC unit cell will be the least integer multiple of *r*. For a rational number *r*, the length of LCPC unit cell would be $p_{LC} = Rp$, where *R* is the least integer multiple of *r*. To make *r* more acceptable, we write $r = R / (R - m)$, where *R* and *m* are both positive integers, and $m < R$. For $r \to 1$ (i.e. $R \to \infty$ and $m = 1$), we shall have broadband slow modes and intensive flat bands inside LCPC [14]. By delicately modulating gain and loss in the LCPC structure, taking the middle plane of the *A* dielectric layer as the origin of the system, we can produce PCs following PT-symmetry. Directed by $n(z) = n^*(-z)$, Fig. 1(b) describes photonic crystals PC_1, PC_2, and LCPC with PT-symmetry. In these configurations, PT-symmetry is satisfied in all constructions, where *A'* and *C'* note for materials with gain and loss, *B'* denotes the same material as *B* (i.e. $n_{B'} = n_B$). The refractive index of dielectric material *A'* and *C'* are $n_{A'} = n_A + i\gamma$ and $n_{C'} = n_A - i\gamma$ with $n_A = 3.46$ (silicon), $n_B = 1$ (air). In this paper, we assume all the dielectric materials as isotropic and dispersionless with permeability $\mu = 1$. All the results in this paper are calculated in TE-polarization while the TM mode can be computed in the same way.

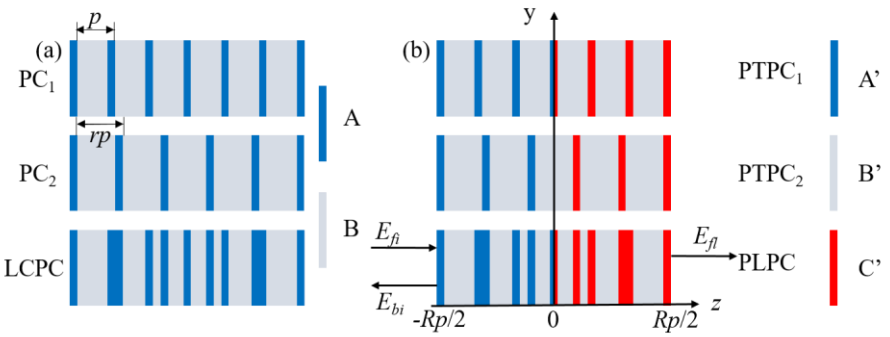

Fig. 1. Schematic illustration of PC_1, PC_2 and LCPC for (a) non-PT-symmetric structure and (b) PT-symmetric configuration.

Usually, we use the transfer matrix method (TMM) to calculate the spectrum of multilayer structures [25]. For every electromagnetic wave propagating along the z-axis, it can be noted by two waves propagating forward and backward:

$$E(z) = E_f(z)\exp(ikz) + E_b(z)\exp(-ikz) \tag{1}$$

where E_f(z) and E_b(z) are the coefficients of the electric field for forward and backward propagating waves, respectively. The transfer matrix of the interface between two different dielectrics can be expressed by:

$$M_{A\to B} = \frac{1}{2}\begin{bmatrix} 1+\frac{k_{Az}}{k_{Bz}} & 1-\frac{k_{Az}}{k_{Bz}} \\ 1-\frac{k_{Az}}{k_{Bz}} & 1+\frac{k_{Az}}{k_{Bz}} \end{bmatrix} \tag{2}$$

where $k_{A(B)z}$ and $d_{A(B)}$ is the wave vector along the z-axis and the thickness respect to the material A or B. Similarly, we can derive $M_{B\to A}$ by simply altering $k_{Az}\to k_{Bz}$. The transfer matrix in the isotropic homogeneous medium is:

$$M_P = \begin{bmatrix} \exp(ik_z d) & 0 \\ 0 & \exp(-ik_z d) \end{bmatrix} \tag{3}$$

Thus, the TMM for LCPC can be given by:

$$\begin{bmatrix} E_{fe} \\ E_{be} \end{bmatrix} = M\begin{bmatrix} E_{fi} \\ E_{bi} \end{bmatrix} = \begin{bmatrix} M_{11} & M_{12} \\ M_{21} & M_{22} \end{bmatrix}\begin{bmatrix} E_{fi} \\ E_{bi} \end{bmatrix} \tag{4}$$

in which $E_{i(e)}$ means the amplitude of waves in the incident (exit) propagation domain. In PT-symmetric systems, the transmission and reflection coefficient for the left (L) and right (R) incident lights is $t = t_L = t_R = 1/M_{22}$, $r_L = -M_{21}/M_{22}$, $r_R = M_{12}/M_{22}$ [21,26]. As we can see, the transmission for both right and left incidence is the same, but the reflection from two opposite directions are entirely different. Following the above discussion, we can write the scattering matrix ($S = [t_L\ r_R;\ r_L\ t_R]$) of the PT-symmetric LCPC. The eigenvalues of the S matrix can be expressed as $s_{1,2} = t \pm \sqrt{r_R r_L}$. By applying generalized conservation relation, the reflectivity and transmittance can be expressed as $|\ T-1\ | = \sqrt{R_R R_L}$ [27], or in other form as $r_R\ r_L{}^* = 1-T$ [28], where $R_{L,R} = |\ r_{L,R}\ |^2$ is the reflectance of the left and right incident lights, and $T = |\ t\ |^2$ is the transmittance of the incident light. Clearly, when $T < 1$, $r_R\ r_L{}^* > 0$, and the phase of r_R and r_L are the same; on the other hand, when $T > 1$, the phase difference between r_R and r_L would be π. Also, $T = 1$ shall lead to $r_R = 0$ or $r_L{}^* = 0$, which is phase transition point, also called exceptional point [27,28]. When exceptional points arise, the eigenvalues of scattering matrix (i.e. $s_{1,2}$) changes from real number to complex number. Then, the unidirectional reflectionlessness locating at EPs will appear.

3. Result and discussion

For the sake of illustration, we plot the index distribution and the normalized Fourier spectrum for PT-symmetric PC_1 ($PTPC_1$), PT-symmetric PC_2 ($PTPC_2$) and PT-symmetric LCPC (PLPC) in Fig. 2. In this figure, p is set as 500 nm, $f_1 = 0.2$ and $R = 6$, $m = 1$. As shown in Fig. 2(a)-(f), the real (imaginary) part of the refractive index for $PTPC_1$, $PTPC_2$ and PLPC are denoted by the solid (dashed) line colored with red, blue and violet, respectively. By taking the middle plane of the LCPC structure ($z = 0$ in Fig. 1(b)) as the origin of the PT-symmetric system, the real part (solid line) of the index obeys even function while the imaginary part (dash-dotted line) behaves as an odd function. Fig. 2(g) shows the Fourier expansion of $PTPC_1$ (red star),

$PTPC_2$ (blue dot) and PLPC (violet triangle) structures in which the period shown in Fig. 1(a) (bottom) is infinitely repeated. Inspecting the Fourier expansion of these three structures, we find that the Fourier spectrum of PLPC is the composition of every ingredient in $PTPC_1$ and $PTPC_2$. In other words, the Fourier components of PLPC consist of most Fourier components that exist in $PTPC_1$ and $PTPC_2$, though with a tiny scale in values of each element. This feature means that the PLPC structure made up of logical "OR" operation possesses the main properties of $PTPC_1$ and $PTPC_2$. Therefore, it is useful to resort to the Fourier spectrum when evaluating the reflection and transmission properties of PLPC. Note that the imaginary part of the refractive index won't affect the Fourier spectrum due to its odd-function distribution. Thus, the Fourier spectrum can be used only in analyzing the influence of the real part of the constituting dielectric materials. However, it does play an instructive role in understanding the PT-symmetric LCPC structure.

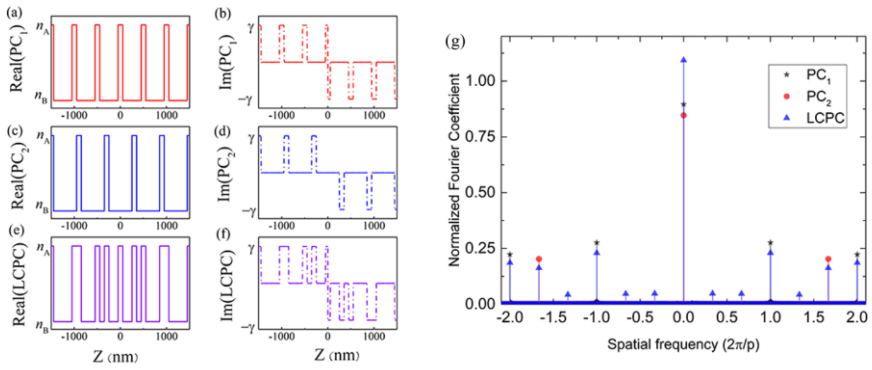

Fig. 2. Dielectric constant distribution of PC_1 (a, b), PC_2 (c, d) and LCPC (e, f) for both real part (solid line) and imaginary part (dash-dotted line). (g) The Fourier expansion for infinite period of $PTPC_1$ (star), $PTPC_2$ (dot) and PLPC (triangle) are shown in the right panel.

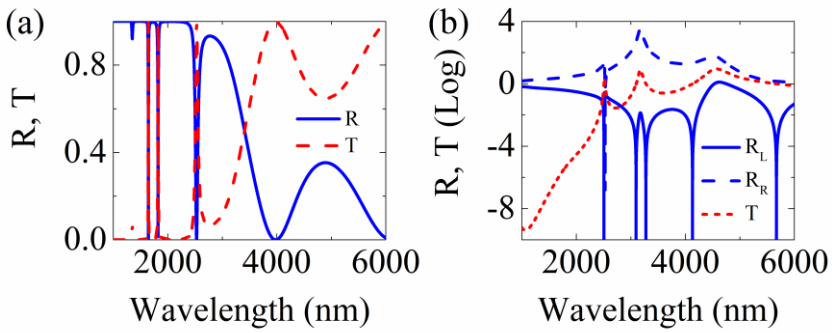

Fig. 3. Reflectivity and transmittance for non-PT-symmetric LCPC (a) and PT-symmetric LCPC (b) structures. The blue line indicates the reflectivity and the red one corresponds to the transmittance.

We calculate the transmittance and reflectivity spectra of LCPC for both non-PT and PT-symmetric structures in Fig. 3. The structural parameters are chosen the same as Fig. 2 and the index is set as $n_A = 3.46$, $n_B = 1$, $\gamma = 1$, the period number of LCPC is $N = 1$. Fig. 3(a) describes the spectrum for non-PT-symmetric LCPC structure, and the result shows that the reflectivity is identical for light incident from opposite directions and the sum of transmittance and reflectivity equals to 1 as expected. The predominant dips (peaks) are caused by the

multiple Bloch coupling inside the LCPC structure [11]. In Fig. 3(b), the reflectivity from the left side is marked by the solid blue line while the dashed blue line corresponds to the opposite case. The transmittance is described by the red dotted line. To observe the reflectivity and transmittance of the PLPC structure clearly, we take the logarithmic operation for R_R, R_L, and T. Apparently, by adding a delicate imaginary modification, the spectrum changes greatly compared with the non-PT one. The non-PT-symmetric counterpart shows an ordinary spectrum with reciprocal features while the PT-symmetric part shows extremely asymmetric reflection for lights incident from different sides. The reflectivity from the right side (gain side) reaches a maximum value of up to 4 orders of magnitude, while on the loss side reflectivity shows the broadband near-zero reflection phenomenon. Furthermore, we see a dip in the reflection spectrum at about λ_i = 2507 nm for light incident from both sides. The main reason for this dip is the interface state generated in the boundary of two materials with an opposite imaginary dielectric constant [29]. As we can see in the following discussions, the electric field mainly concentrates on the interface for wavelength locating at 2507 nm. In Fig. 3(b), a broadband near-zero reflection can be found from 3000 to 4200 nm, in which R_L is always below 0.02, and the average reflectivity is less than 0.01. Compared with the reflectivity from the right side with a quantity as high as $10^3 \sim 10^4$, the reflectivity from the left side is indeed ignorable. Thus, we call this negligible reflectivity as near-zero reflection. Retrieving works related to unidirectional invisibility, most of them are caused by a single EP and the zero reflection wavelength range is very narrow, which limits the potential application of invisibility generated by PT-symmetry. On the contrary, the proposed PLPC structure showing broadband zero reflection might have bright potential in many fields.

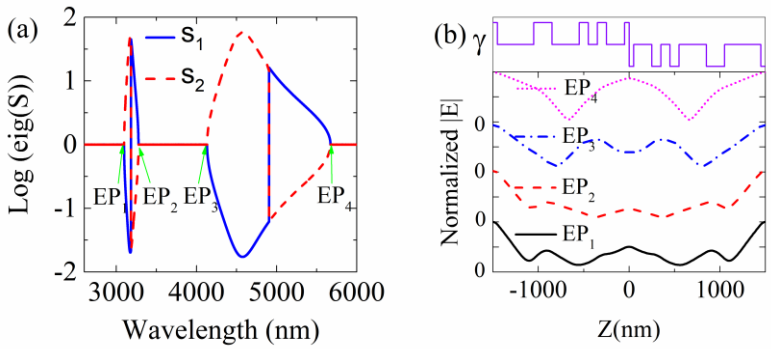

Fig. 4. (a) Eigenvalues ($s_{1,2}$) of S matrix derived by the result of the transfer matrix as a function of wavelength. Four EPs are marked by the green arrows. (b) Electric field inside the PT-symmetric geometry respect to four EPs.

The S matrix is calculated to investigate the PT-symmetric properties of the proposed structure. As shown in Fig. 4(a), two eigenvalues of the S matrix are plotted, which is denoted by s_1 and s_2, respectively. The eigenvalues of the S matrix of PT-symmetric structure either form pairs with reciprocal moduli or they are all in unit modulus [21]. The unit modulus means the PT-symmetric phase while the reciprocal moduli indicate the PT-broken phase. By taking the logarithm of each eigenvalue, we can get a symmetrical graphic along the x-axis. The EPs noted by four green arrows are marked as EP_i (i = 1, 2, 3, 4), with values EP_1 = 3098 nm, EP_2 = 3277 nm, EP_3 = 4133 nm and EP_4 = 5673 nm, respectively. Each EP corresponds to a deep reflection dip depicted in Fig. 3(b). As we have discussed above, the first dip locating at λ_i = 2507 nm is caused by the interface state generated by two materials with the opposite imaginary part. Between EP_1 and EP_3, there exists a broad band showing no reflection. In fact, the accurate zero reflection of the left incidence can only be caused by the EPs. However, by designing structures properly, when the EP pairs of the PT-symmetric device sit nearby, the broadband near-zero reflection is expected to appear by suppressing the laser mode generated

by the phase jump inside the EP pairs, which can be called as quasi-laser mode here. As EP pair could possess quasi-laser mode inside it (for example, quasi-laser$_1$ inside EP$_1$ and EP$_2$, and quasi-laser$_2$ between EP$_3$ and EP$_4$), the reflectivity from the loss side would encounter an enhancement at wavelengths correspond to the quasi-laser modes. But as the EPs sit nearby, the enhancement of the reflectivity caused by the quasi-laser mode is suppressed. This is also the reason why the BNZR stops at EP$_3$ instead of EP$_4$.

To further investigate the underlying physics of the BNZR phenomenon, we plot the normalized electric distribution inside the geometry at the frequencies of EP$_1$, EP$_2$, EP$_3$, and EP$_4$, respectively. The intensity profile is calculated in one period PLPC unit cell. As shown in Fig. 4(b), the upper panel depicts the imaginary part of the index distribution of the PLPC structure. And the normalized electrical amplitudes equal to 1 outside the structure. Clearly, the intensity profile is spatially symmetric along the z-axis due to the parity-time symmetry. Assume $E(z)$ is the electric distribution of a left incident wave, then at the PT operation, $E^*(-z)$ is also a left incident wave of the same frequency. They must be identical (up to a phase φ) by the requirement of uniqueness: $E*(-z) = e^{i\varphi}E(z)$ [27]. Hence, the electric intensity $I(z) = |E(z)|^2 = I(-z)$. Therefore, the intensity profile at EPs obeys even function. It's worth noting that for all PT-symmetric structures, the energy flow inside the PT-symmetric structure always goes from gain side to loss side [30]. Thus, standing waves and multiple resonances could be generated in the geometry, leading to further absorption in the lossy layers.

The interface state occurring at the interface of two materials with the opposite imaginary part is also investigated. As shown in Fig. 5(a), the normalized electric field for the interface state is plotted. The PLPC structure stretch from -1500 nm to 1500 nm and the dielectric outside the structure is air with index 1. The electric field inside the geometry decays exponentially from the origin towards both sides. Similar wave localization of the interface effect can also be observed in PLPC with more units. The interface state exists in the boundary of two PCs with real permittivity is called optical Tamm state, which results from the sign change of surface impedance of PCs across the interface [31]. Similarly, the sign change of the imaginary parts of permittivity can also lead to interface state [29]. It's worthy to note that the interface state generated in PT-symmetric structures will also lead to the change of the eigenvalues, as shown in Fig. 5(b). Like EPs, the interface state would result in an abrupt phase change at the corresponding frequency, and the discontinuity at λ = 2512 nm is caused by the phase jump of reflection coefficients. However, comparing Fig. 4(b) and Fig. 5(a), we can find that for EPs, the electric field in the structure is much lower than that of interface state. Thus, the main difference between the interface state and EP would be the electric intensity inside the structure.

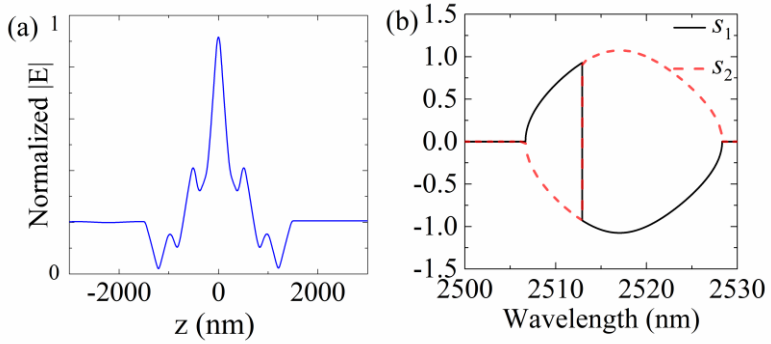

Fig. 5. (a) Electric field of interface state inside the PT-symmetric geometry. (b) Eigenvalues of the *S* matrix as a function of wavelength respect to the interface state.

Furthermore, we compared the spectral properties of the periodic PT-symmetric structures ($PTPC_1$ and $PTPC_2$) with the aperiodic PLPC structure. As plotted in Fig. 6, the reflectivity of the $PTPC_1$, $PTPC_2$ and PLPC structures are indicated by the solid black line, dash red line, and dash-dotted blue lines in Fig. 6(a). All the structures are calculated at a length of 3000 nm. For conciseness, we show the wavelength range from 3000 nm to 4200 nm where the BNZR phenomenon appears. Apparently, the reflectivity of the PLPC structure is much lower than that of $PTPC_1$ and $PTPC_2$ in this broad wavelength range. The average reflectivity of PLPC is 0.01 over this band with a maximum reflectivity equals to 0.02 locating at 3735 nm. But for periodic configurations $PTPC_1$ and $PTPC_2$, the average reflectivity equals 0.11 and 0.12 and the maximum reflectivity is 0.26 and 0.34, respectively. Thus, by applying the logical configuration to periodic PCs, the reflectivity magnitude decreases over 10 times. In Fig. 6(b), we plot the logarithmic eigenvalues of the *S* matrixes correspond to $PTPC_1$, $PTPC_2$, and PLPC structures. For $PTPC_1$, EPs locate at 3254 nm and 3593 nm, the former EP corresponds to the zero reflectivity of right side (gain) incidence, while the latter one corresponds to the reflectionlessness of left side (loss) incidence. Thus, the interaction of EPs can't play the role in suppressing the reflection. Similarly, for $PTPC_2$, the EPs also correspond to zero reflection from different sides. However, for PLPC, EP_1, EP_2, and EP_3 all correspond to the zero reflectivity from the loss side, which plays a vital role in inhibiting the reflection, causing the BNZR phenomenon.

EP点对应相同方向无反射才可以压制一段频率反射

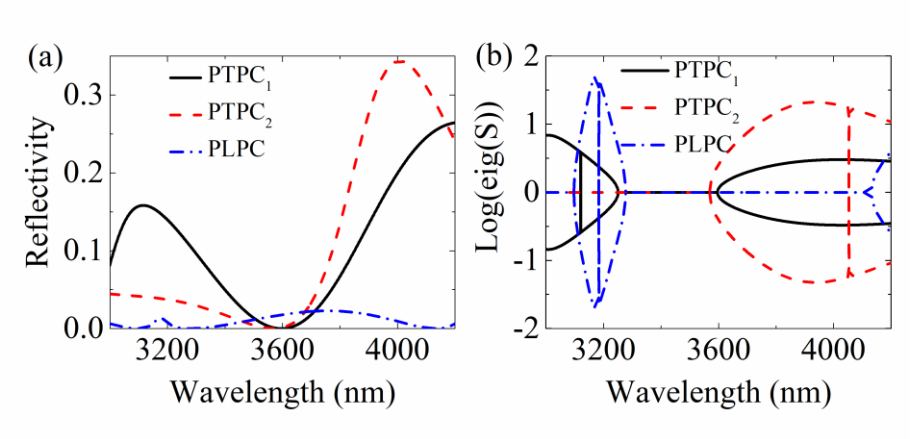

Fig. 6. (a) The comparison of reflectivity of the PT-symmetric structure composed by periodic and aperiodic configuration. (b) Eigenvalues of *S* matrix corresponding to periodic PT-symmetric structure and aperiodic PT-symmetric counterpart.

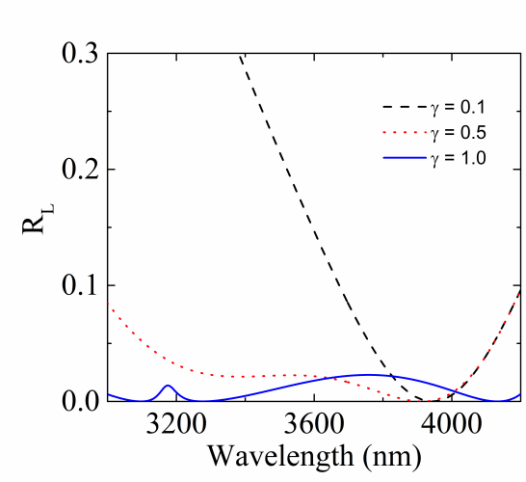

Fig. 7. The reflectivity of the left incident wave (R_L) with various γ.

In Fig. 7, we calculated the reflectivity of the left incident wave (R_L) with various γ. The black dashed line, the red dotted line, and the solid blue line correspond to the reflectivity of γ = 0.1, γ = 0.5, and γ = 1, respectively. Here, to directly demonstrate our idea of BNZR in a relatively simple PT-symmetric structure, a large value of loss/gain γ = 1.0 is selected [32], though it is difficult to realize in practice. A large γ would produce more EPs in PCs, making the BNZR phenomenon more pronounced. If this loss/gain value is reduced (e.g., γ = 0.1 and γ = 0.5), the broadband near-zero reflection will gradually disappear (see Fig. 7) owing to weak wave scattering in the proposed structure. This problem might be figured out using other LCPC structures or other non-Hermitian media [33–35] and we will do further study on it in the future.

4. Conclusion

In summary, we propose a broadband near-zero reflection phenomenon generated in the PT-symmetric LCPC structure. The broadband may reach 1200 nm or more from 3000 to 4200 nm, with the average reflectivity below 0.01 and the maximum value less than 0.02. The Fourier expansion of the refractive index shows the logical combined photonic crystal possesses most of the properties of the periodic PC, but the spectrum of the PLPC structure shows many differences compared with the periodic ones. We calculated the scatter matrix and find that the BNZR is revealed by EPs suppressing the enhancement of the reflectivity. The electric field distribution respect to the EPs inside the geometry obeys even functions to the origin. The multiple Bloch modes in periodic photonic crystals are expected to couple with each other in the PT-symmetric LCPC, inducing interesting properties undiscovered in other structures, which deserves further discussion. Also, note that the ideal symmetry-breaking transition will not appear in PT-symmetric materials with strong dispersion owing to the causality principle [36], therefore we assume the PT-symmetric PCs are non-dispersive in this work, which is more straightforward to study the broadband unidirectional near-zero reflection relevant to EPs. Although the frequency dependence is forbidden in PT-symmetric materials, quasi-PT symmetry [33,34] or medium with Kramers–Kronig relations [35] is a good candidate to study the dispersion behavior, which might be a more practical way to access broadband unidirectional reflection. For what it's worth, our proposed concept of LCPC with PT-symmetry may lead to more study on non-Hermitian media with logical operation and the proposed broadband unidirectional reflection effect can find application in broadband photonic spin Hall effect [37] and broadband sensing.

Acknowledgment

This work was supported by the National Natural Science Foundation of China (Grant Nos. 11904169 and 61675095), the Natural Science Foundation of Jiangsu Province (Grant No. BK20190383), and the Foundation of Graduate Innovation Center in NUAA (Grant No. kfjj20170802).

Disclosures

The authors declare no conflicts of interest.

References

1. J. D. Joannopoulos, "Photonic crystals: putting a new twist on light," Nature **386**, 143–149 (1997).
2. A. Yariv and P. Yeh, Optical Waves in Crystals: Propagation and Control of Laser Radiation, Wiley Series in Pure and Applied Optics (Wiley, 1984).
3. Toshihiko Baba, "Slow light in photonic crystals," Nat. Photonics **2**(8), 465-473 (2008).

4. F. Wang, Y. Z. Cheng, X. Wang, Y. N. Zhang, Y. Nie, and R. Z. Gong, "Narrow Band Filter at 1550 nm Based on Quasi-One-Dimensional Photonic Crystal with a Mirror-Symmetric Heterostructure," Materials **11**(7), 1099 (2018).
5. D. Headland, X. Yu, M. Fujita, and T. Nagatsuma, "Near-field out-of-plane coupling between terahertz photonic crystal waveguides," Optica **6**(8), 1002 (2019).
6. J. Noh, W. A. Benalcazar, S. Huang, M. J. Collins, K. P. Chen, T. L. Hughes, and M. C. Rechtsman, "Topological protection of photonic mid-gap defect modes," Nat. Photonics **12**(7), 408–415 (2018).
7. E. Maciá, "Exploiting aperiodic designs in nanophotonic devices," Rep. Prog. Phys. **75**(3), 036502 (2012).
8. D. Levine and P. J. Steinhardt, "Quasicrystals: A New Class of Ordered Structures," Phys. Rev. Lett. **53**(26), 2477–2480 (1984).
9. M. Kohmoto, B. Sutherland, and K. Iguchi, "Localization of optics: Quasiperiodic media," Phys. Rev. Lett. **58**(23), 2436–2438 (1987).
10. L. Dal Negro and S. V. Boriskina, "Deterministic aperiodic nanostructures for photonics and plasmonics applications," Laser Photonics Rev. **6**(2), 178–218 (2012).
11. G. Alagappan and C. E. Png, "Broadband slow light in one-dimensional logically combined photonic crystals," Nanoscale **7**(4), 1333–1338 (2015).
12. A. M. Vyunishev, P. S. Pankin, S. E. Svyakhovskiy, I. V. Timofeev, and S. Ya. Vetrov, "Quasiperiodic one-dimensional photonic crystals with adjustable multiple photonic bandgaps," Opt. Lett. **42**(18), 3602–3605 (2017).
13. Y. Fei, Y. Liu, D. Dong, K. Gao, S. Ren, and Y. Fan, "Multiple adjustable optical Tamm states in one-dimensional photonic quasicrystals with predesigned bandgaps," Opt. Express **26**(26), 34872~34879 (2018).
14. G. Alagappan and C. E. Png, "Flat bands of optical dielectric beats," J. Opt. Soc. Am. A **35**(5), 794–797 (2018).
15. C. E. Rüter, K. G. Makris, R. El-Ganainy, D. N. Christodoulides, M. Segev, and D. Kip, "Observation of parity–time symmetry in optics," Nat. Phys. **6**(3), 192–195 (2010).
16. C. M. Bender and S. Boettcher, "Real Spectra in Non-Hermitian Hamiltonians Having P T Symmetry," Phys. Rev. Lett. **80**(24), 5243–5246 (1998).
17. Z. H. Musslimani, K. G. Makris, R. El-Ganainy, and D. N. Christodoulides, "Optical solitons in PT periodic potentials," Phys. Rev. Lett. **100**(3), 030402 (2008).
18. K. G. Makris, R. El-Ganainy, D. N. Christodoulides, and Z. H. Musslimani, "Beam Dynamics in P T Symmetric Optical Lattices," Phys. Rev. Lett. **100**(10), 103904 (2008).
19. Y. Fu and Y. Xu, "Asymmetric effects in waveguide systems using PT symmetry and zero index metamaterials," Sci. Rep. **7**(1), 12476 (2017).
20. Y. Fu, X. Zhang, Y. Xu, and H. Chen, "Design of zero index metamaterials with PT symmetry using epsilon-near-zero media with defects," J. Appl. Phys. **121**(9), 094503 (2017).
21. Z. Lin, H. Ramezani, T. Eichelkraut, T. Kottos, H. Cao, and D. N. Christodoulides, "Unidirectional Invisibility Induced by P T -Symmetric Periodic Structures," Phys. Rev. Lett. **106**(21), 213901 (2011).
22. L. Feng, Y.-L. Xu, W. S. Fegadolli, M.-H. Lu, J. E. B. Oliveira, V. R. Almeida, Y.-F. Chen, and A. Scherer, "Experimental demonstration of a unidirectional reflectionless parity-time metamaterial at optical frequencies," Nat. mater. **12**, 6 (2013).
23. X.-Y. Zhu, Y.-L. Xu, Y. Zou, X.-C. Sun, C. He, M.-H. Lu, X.-P. Liu, and Y.-F. Chen, "Asymmetric diffraction based on a passive parity-time grating," Appl. Phys. Lett. **109**(11), 111101 (2016).
24. X.-F. Zhu, "Defect states and exceptional point splitting in the band gaps of one-dimensional parity-time lattices," Opt. Express **23**(17), 22274 (2015).
25. P. Markoš and C. M. Soukoulis, Wave Propagation: From Electrons to Photonic Crystals and Left-Handed Materials (Princeton University Press, 2008).
26. A. Mostafazadeh, "Spectral Singularities of Complex Scattering Potentials and Infinite Reflection and Transmission Coefficients at Real Energies," Phys. Rev. Lett. **102**(22), 220402 (2009).
27. L. Ge, Y. D. Chong, and A. D. Stone, "Conservation relations and anisotropic transmission resonances in one-dimensional PT -symmetric photonic heterostructures," Phys. Rev. A **85**(2), 023802 (2012).
28. Y. Fu, Y. Xu, and H. Chen, "Zero index metamaterials with PT symmetry in a waveguide system," Opt. Express **24**(2), 1648 (2016).
29. X. Cui, K. Ding, J.-W. Dong, and C. T. Chan, "Exceptional points and their coalescence of PT -symmetric interface states in photonic crystals," Phys. Rev. B **100**(11), 115412 (2019).
30. R. Fleury, D. L. Sounas, and A. Alù, "Negative Refraction and Planar Focusing Based on Parity-Time Symmetric Metasurfaces," Phys. Rev. Lett. **113**(2), 023903 (2014).
31. A. V. Kavokin, I. A. Shelykh, and G. Malpuech, "Lossless interface modes at the boundary between two periodic dielectric structures," Phys. Rev. B **72**(23), 233102 (2005).
32. K. Ding, Z. Q. Zhang, and C. T. Chan, "Coalescence of exceptional points and phase diagrams for one-dimensional P T -symmetric photonic crystals," Phys. Rev. B **92**(23), (2015).
33. D. M. Tsvetkov, V. A. Bushuev, V. V. Konotop, and B. I. Mantsyzov, "Broadband quasi- PT -symmetry sustained by inhomogeneous broadening of the spectral line," Phys. Rev. A **98**(5), 053844 (2018).
34. V. A. Bushuev, D. M. Tsvetkov, V. V. Konotop, and B. I. Mantsyzov, "Unidirectional invisibility and enhanced reflection of short pulses in quasi-PT-symmetric media," Opt. Lett. **44**(23), 5667 (2019).
35. T. G. Philbin, "All-frequency reflectionlessness," J. Opt. **18**(1), 01LT01 (2016).
36. A. A. Zyablovsky, A. P. Vinogradov, A. V. Dorofeenko, A. A. Pukhov, and A. A. Lisyansky, "Causality and phase transitions in PT -symmetric optical systems," Phys. Rev. A **89**(3), 033808 (2014).

37. Y.-Y. Fu, Y. Fei, D.-X. Dong, and Y.-W. Liu, "Photonic spin Hall effect in PT symmetric metamaterials," Front. Phys. **14**(6), 62601 (2019).